5.
THIN PROFILE WIDEBAND PRINTED MONOPOLE ANTENNA FOR SLIM MOBILE HANDSET APPLICATIONS

5.1 Introduction

To achieve the various communication frequency bands in a single antenna, several multiband/wideband antennas for mobile handsets applications have been reported, like inverted-F antenna (IFA) [Lee and Sung (2014), Seko and Correra (2013), Chien and Chi (2009)], planar inverted-F antenna [Karkkainen (2005), Yoon and Park (2007), Rowell and Murch (1997), Chien *et al*. (2004), Montaser (2015), Seol *et al*. (2007), Chattha and Huang (2011), Chang and Wong (2009), Wong and Huang (2008)], and folded loop with chip element (inductor and capacitor) antennas [Chi and Wong (2008), Wong and Kang (2008), Li and Wong (2010), Wong and Lee (2010), Wong *et al*. (2010)]. Although both IFA and PIFA are multiband compact antennas with quarter wavelength structure, suitable for conventional mobile handsets, but exhibit additional height in addition to the substrate thickness which gives system design complexity. The radiating structures of folded chip antennas consist of multiple layers. These layers are connected through shorting pin. The adjustment of the multiple layers inside the mobile phone is complicated because adjustment of gap between multiple layers is a difficult task for antenna designers. In addition to this, to make compact geometry, antenna is loaded with chip element such as capacitor and inductor which bring the losses. Due to the chip element, the total radiated power decreases which results in decrease in radiation efficiency.

On the other hand, the planar monopole antennas are one of the preferable candidates for slim mobile handsets. The planar monopole antenna is quarter wavelength resonating structure which can be easily etched during the fabrication of printed circuit board (PCB) of mobile phones.

Some of the monopole antennas are studied to obtain the different wireless communication bands including next generation communication bands [Chen *et al*. (2008), Zhang *et al*. (2011), Chen *et al*. (2009), Bharti *et al*. (2014), Chen and

Wong (2011), Chen and Wong (2010), Zhao *et al*. (2013)]. In [Chen *et al*. (2008)], two inverted-L branches and an open stub are studied for impedance tuning to achieve the GSM900 and DCS/PCS/UMTS frequency bands. Zhang *et al.* [Zhang *et al*. (2011)], discussed monopole antenna, which consists of two-strip monopole and a meandered strip which covers GSM850/900 and GSM1800/1900/UMTS/ LTE2300/2500 frequency bands. In [Chen *et al*. (2009)], quad band compact printed monopole antenna is demonstrated for GSM900/DCS/PCS/WLAN applications. In [Bharti *et al*. (2014)], a compact multi band planar monopole antenna is proposed for slim mobile handset applications which operate over GSM900/1800/1900/UMTS/IMT2100/ WLAN/ LTE2500/WiMAX frequency bands. The above reported monopole antennas in [Chen *et al*. (2008), Zhang *et al*. (2011), Chen *et al*. (2009)], operate over the GSM850/900 frequency band at lower frequency and covers most of the wireless communication bands at higher frequency except WiMAX. Further effort has been made for widening the lower operating band to cover LTE700 along with GSM850/900 band [Chen and Wong (2011), Chen and Wong (2010), Zhao *et al*. (2013)]. Coupled feed PIFA [Chen and Wong (2011), Chen and Wong (2010)] were used for widening the lower operating frequency band in addition to the higher operating frequency bands. However, these antennas utilize some height from the substrate and occupy a larger area. Therefore, these are not suitable for the slim mobile handsets. Also, WiMAX frequency band is still not covered within above studies.

In this chapter, a low profile wideband printed monopole antenna is proposed. The proposed antenna operates over the LTE700/GSM850/900/ GPS L1/GSM1800/1900/UMTS/IMT2100/Wi-Fi/LTE2300/2500, and WiMAX frequency bands based on –6 dB reflection coefficients. The simulated and measured results are found in good agreement. The configuration of the proposed antenna consists of two strips named as coupling strip and shorted radiating strip at top of the substrate, whereas meandered parasitic strip at bottom of the substrate. The bottom meandered strip helps in widening the overall operating bands by increasing the capacitance between the main radiating strip and

meandered parasitic strip. The proposed antenna is elaborated through *S*-parameters analysis including typical shape parameters, surface current distributions, and radiation performances. Further, study is carried out in the vicinity of the mobile environment. The antenna configuration and design, antenna characterization in free space as well in the mobile environment are presented in the following sections.

5.2 Antenna Configuration and Design

The proposed antenna is designed on 0.8 mm thick FR4 substrate of dielectric constant 4.4 and loss tangent 0.018. The size of board is chosen 110×50 mm^2 as mobile circuit board. The printed antenna is deposed on the top of the mobile circuit board of footprint 15 × 50 mm^2. The front and rear view of the proposed antenna along with the fabricated prototype is shown in Fig. 5.1(a). The radiating element is placed on front side as well as rear side of the substrate on the no ground portion. The ground plane is also printed on the rear side of the substrate. The coupling and shorting radiating strips are placed on front side whereas meandered line parasitic strip is placed on rear side of the substrate. The details of the front side and rear side radiating elements are shown in Fig. 5.1(b) and Fig. 5.1(c), respectively.

Further, the design concept of the proposed antenna is illustrated with the help of Fig. 5.2. The antenna design starts with a conventional rectangular monopole antenna fed with a 50 Ω microstrip line (Conf 1) which shows dual band characteristics about 1.2 GHz and 2.4 GHz. The dual band behaviour is observed due to the two branches of the 'T' shaped radiator. After that the direct feed is replaced by coupled fed (Conf 2). Since the two branches of the T shaped radiator is replaced by coupled element and driven element, which results in more matching towards higher frequency band while the lower frequency band disturbs and shifts towards higher frequency side with reduced bandwidth.

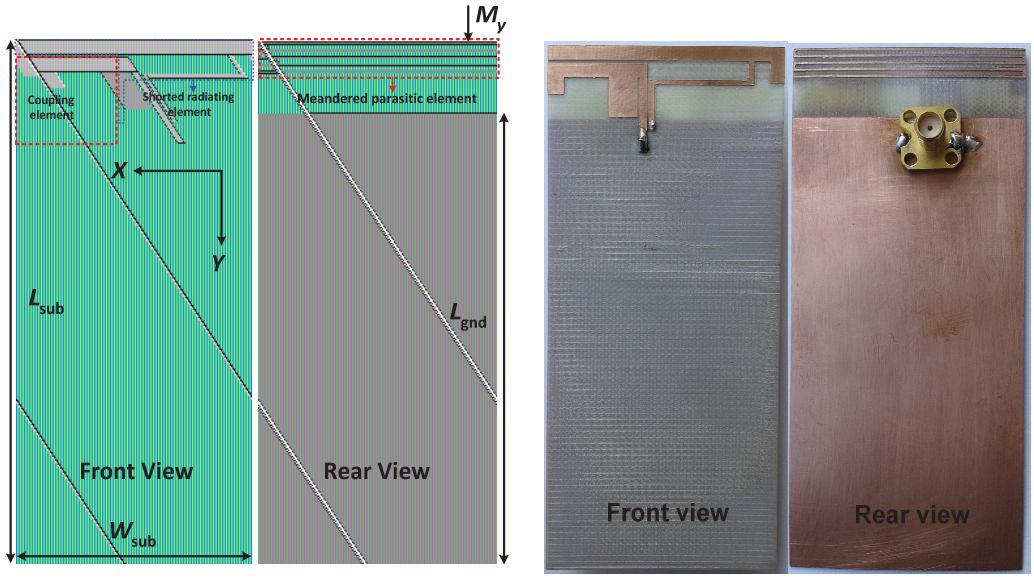

(a)

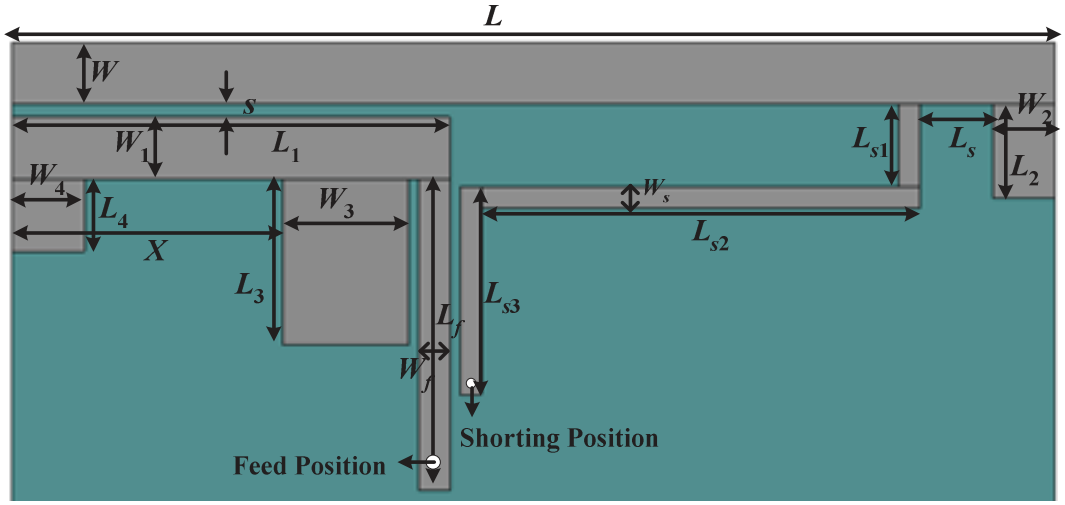

(b)

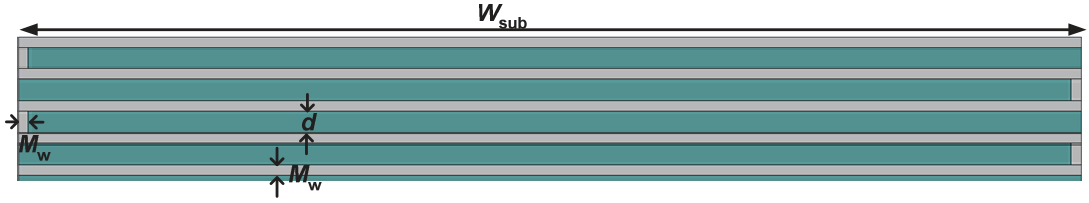

(c)

Fig. 5.1: (a) Front and rear view of the proposed antenna, (b) Details of front side radiating element (c) Details of rear side parasitic meandered strip.

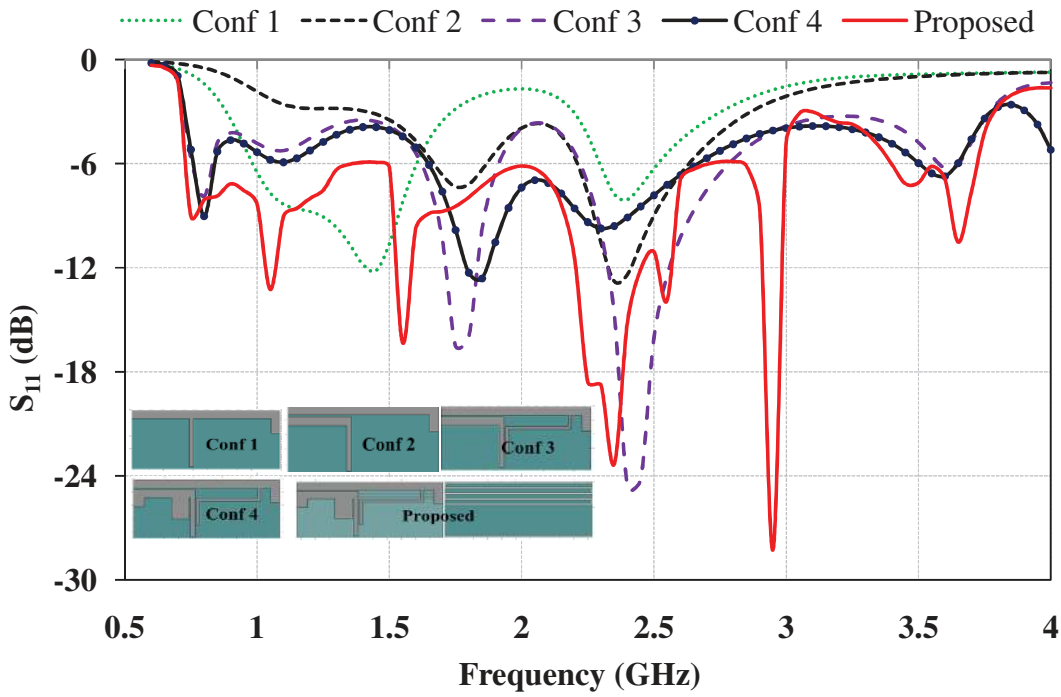

Fig. 5.2: The variation of the reflection coefficient with frequency for different configurations during evolution.

After that, a shorting strip is added to the radiating strip of coupled fed monopole antenna (Conf 3) which results in an additional resonating frequency band about 0.77 GHz towards lower frequency side while matching improves at higher frequency bands about 1.7 GHz and 2.4 GHz. The lower resonant frequency of the proposed antenna can be approximated as,

$$f_r = \frac{c}{\lambda_{eff}}$$

$$\lambda_{eff} \approx \frac{8*(\text{Length of the radiating strip + Length of shorting strip})}{\varepsilon_{eff}}$$

$$\varepsilon_{eff} = \frac{\varepsilon_r + 1}{2}$$

Length of radiating strip = L + L_2

Length of The shorting strip = L_{s1}+ L_{s2}+ L_{s3}

In Conf 4, two tuning stubs are added to the driven elements to tune the impedance bandwidth. Thus, the impedance matching improves significantly about 2 GHz which results in a wideband from 1.6 GHz to 2.7 GHz with respect to –6 dB reflection coefficient. Impedance matching about 0.77 GHz and 3.6 GHz improve due to these stubs. Further, a meandered line parasitic strip is placed on the rear side of the substrate below the antenna to form the proposed optimized antenna that operates in wideband from 0.73 GHz to 3.0 GHz along with coverage of WiMAX band from 3.3 GHz to 3.7 GHz. The parasitic element below the antenna structure can accommodate multiple resonating modes along with the main antenna structure which results in the wideband operations having multiple resonances and most of the important communication bands such that LTE700/GSM800/900 (0.742 GHz–1.36 GHz), GPSL1/GSM1800/1900/UMTS/ IMT2100/Wi-Fi/ LTE2300/2500 (1.475 GHz–2.7 GHz) and WiMAX (3.4 GHz–3.72 GHz).

5.3 Antenna Characterization in Free Space

All the simulations of the proposed antenna are performed originally in finite element method (FEM) based Ansoft's high frequency structure simulator (HFSS) to optimize the antenna shape parameters for the desired operating bands. The optimized shape parameters of the proposed antenna are shown in Table 5.1. After that, the optimized antenna is fabricated using T-Tech QC5000 micro-milling machine. The simulated results of the antenna are validated with finite integration technique (FIT) based simulation software CST Microwave Studio (CST MWS) [26] and measured results.

5.3.1 S-Parameter Characterization

The reflection coefficient variation of the proposed antenna with frequency in free space is shown in Fig. 5.3. It is observed that the measured and simulated results are in good agreement while some discrepancies are observed which may be due to fabrication imperfection. The measured results show that antenna

operate over prerequisite 0.742 GHz–1.36 GHz, 1.475 GHz–2.7 GHz and 3.4 GHz–3.72 GHz frequency bands with –6 dB reflection coefficient.

Table 5.1: Optimized shape parameters of the proposed antenna.

Parameters	Value (mm)	Parameters	Value (mm)
W_{sub}	50	L_s	3.5
L_{sub}	110	L_{s1}	4
L_{gnd}	95	L_{s2}	21
L	50	L_{s3}	10
W	3	s	0.6
L_1	21	X	13
W_1	3	W_f	1.5
L_2	5.65	L_f	15
W_2	3	d	1
L_3	8	W_w	0.5
W_3	6	M_y	0
L_4	3.5	Feed Position	(29.75, 19.6)
W_4	3.7	Shorting Position	(28, 16.5)

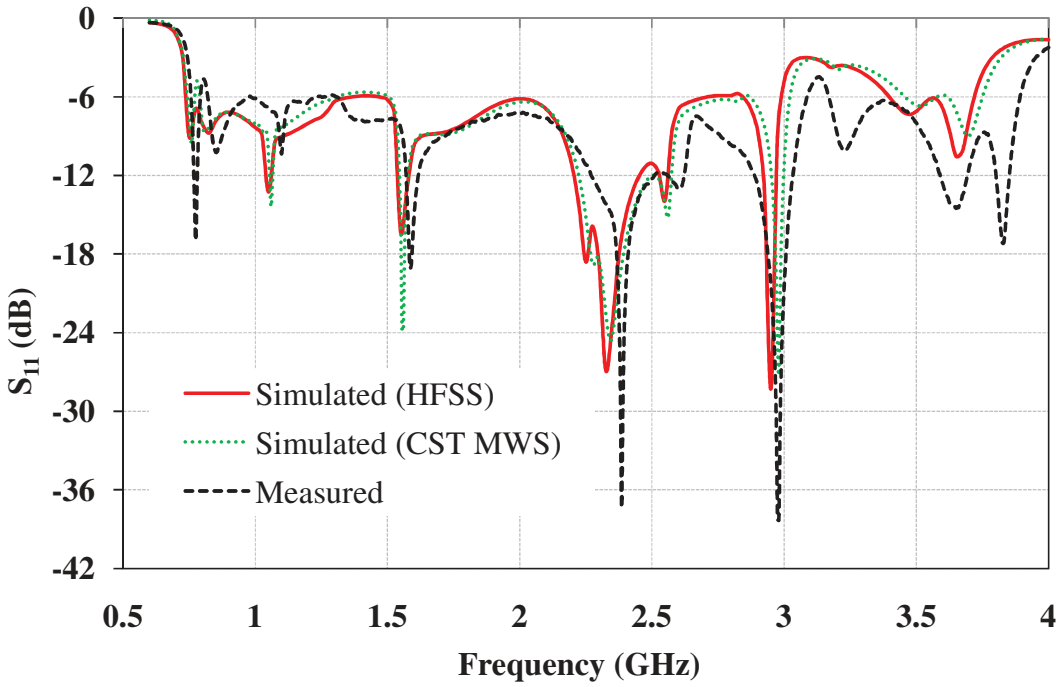

Fig. 5.3: Simulated and measured reflection coefficient.

5.3.2 Parametric Analysis

Parametric analysis of some critical dimensions/shapes of the antenna is carried out to analyse the effect of the shape parameters on the operating frequency bands using HFSS. The variation of the separation '*s*' between the driven and coupled elements on impedance bandwidth is shown in Fig. 5.4. It is observed that impedance matching affect all over the frequency band. For s = 0.9 mm impedance matching is improved about all the frequency bands with some significant mismatch about GSM850 band whereas for s = 0.3 mm impedance matching gets deteriorated significantly towards lower frequency bands as well as WiMAX band therefore the optimized value is taken as 0.6 mm. The effect of variation of the position of shorting strip connection position at the coupled strip L_{s2} on impedance bandwidth is shown in Fig. 5.5. It is observed that impedance matching significantly affected about GSM850 and WiMAX bands due to L_{s2} variation. With decrease of the L_{s2} matching improves towards lower frequency side while deteriorate at higher frequency side. Further, the position of the meandered parasitic element position (M_y) is carried out and observed that it plays significant role on the impedance matching which is shown in the Fig. 5.6. It is observed that when the meandered line shifts from the top position impedance matching gets disturbed while at the extreme top position wideband characteristics is observed. The gap between the horizontal arms of the meandered line is another important parameter which plays significant role in the impedance matching. With the increase of gap between the horizontal arms of the meandered line the impedance matching towards higher frequency decreases with some improvement towards lower frequency side for the d = 1 mm wide impedance matching is observed in Fig. 5.7.

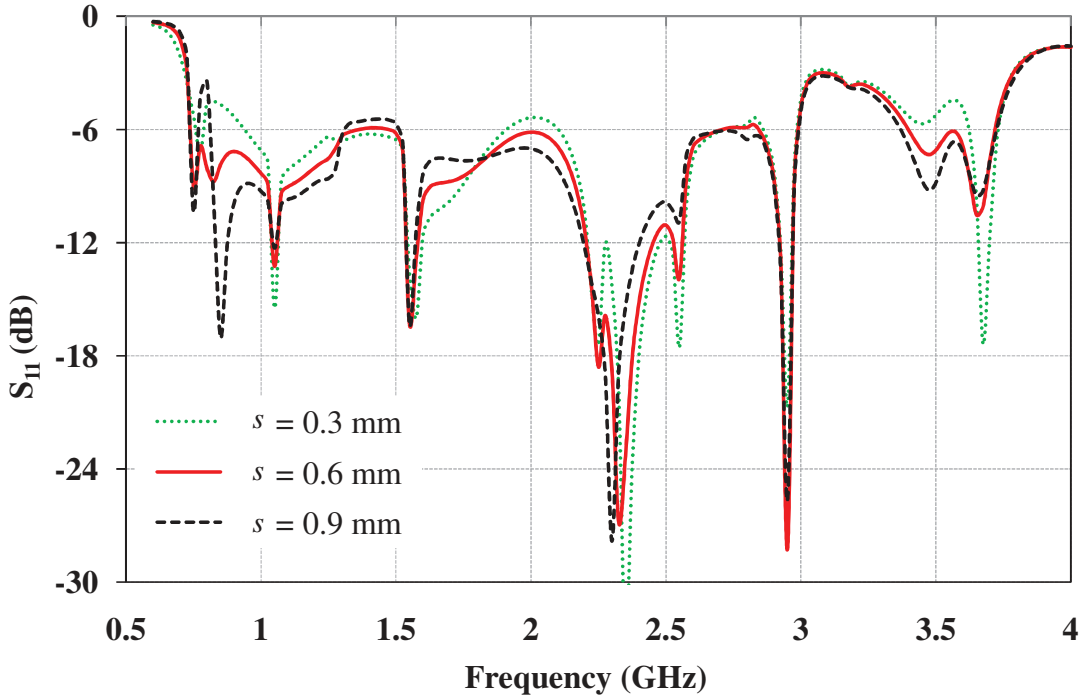

Fig. 5.4: Variation of the reflection coefficient with shape parameter '*s*'.

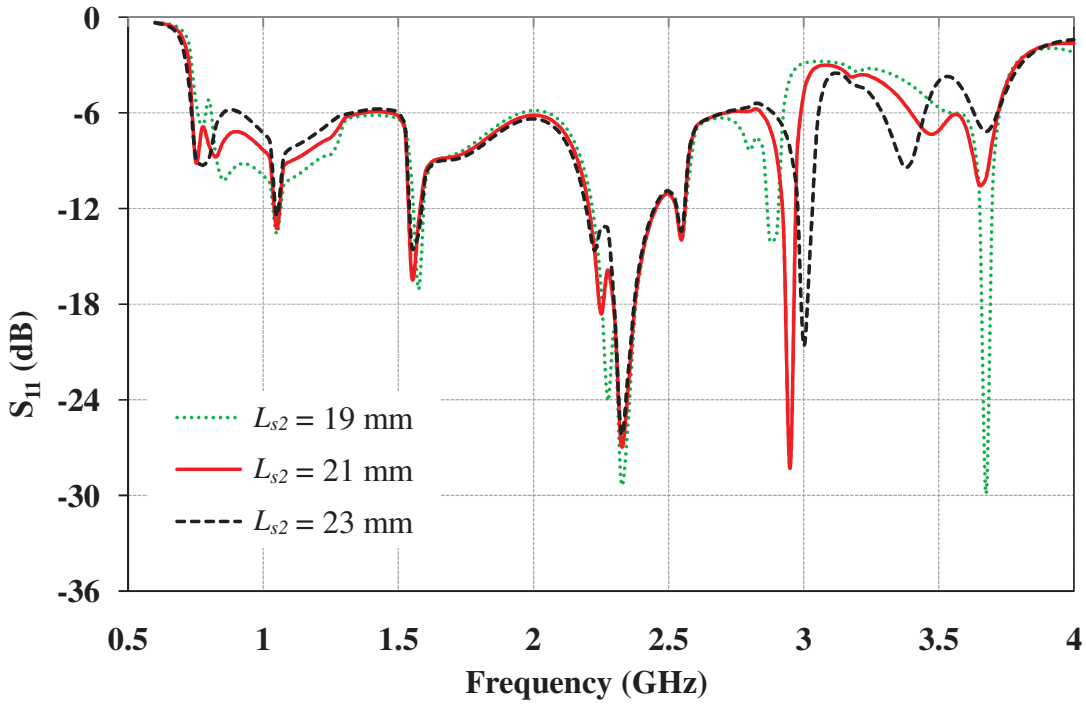

Fig. 5.5: Variation of the reflection coefficient with shape parameter 'L_{s2}'.

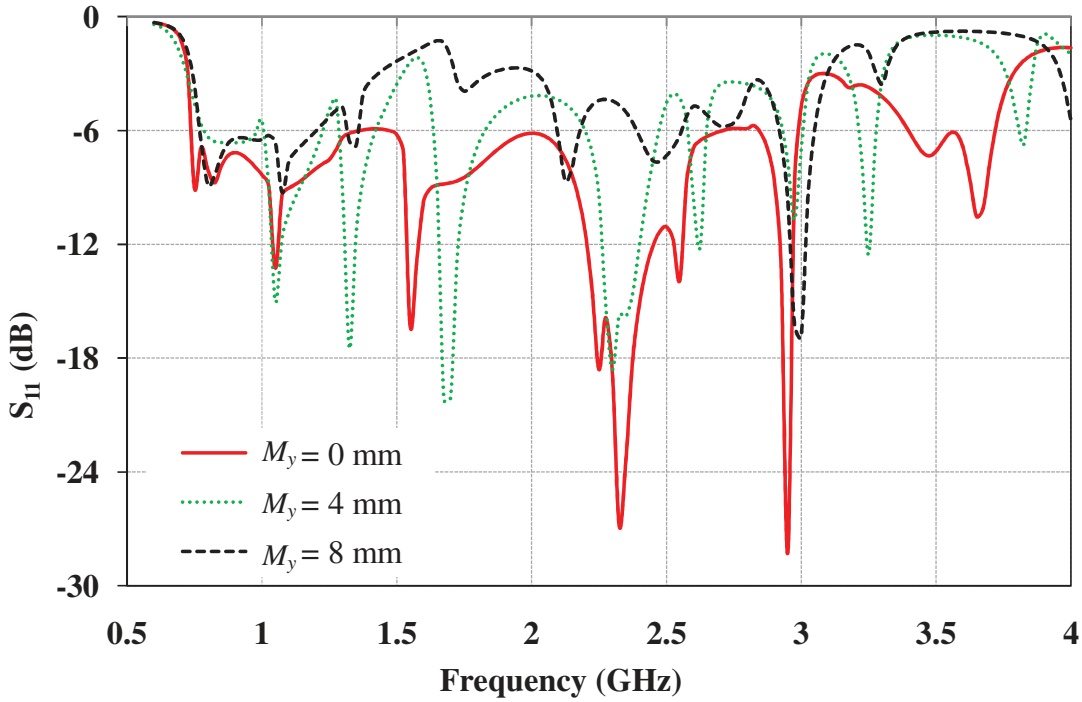

Fig. 5.6: Variation of the reflection coefficient with shape parameter 'M_y'.

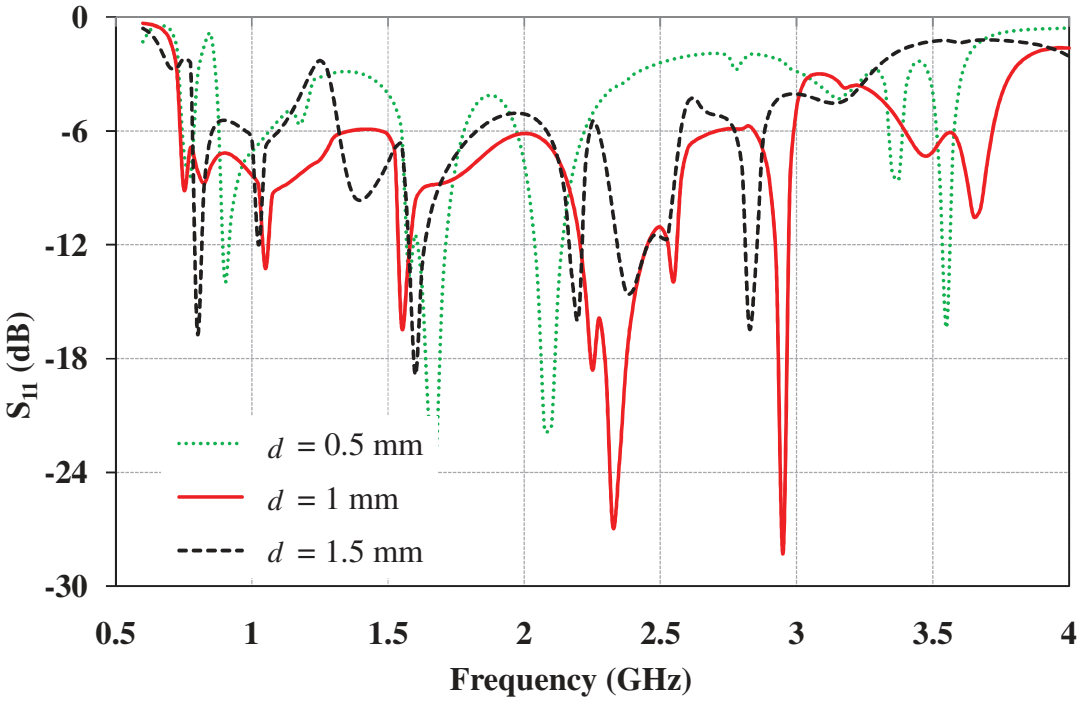

Fig. 5.7: Variation of the reflection coefficient with shape parameter 'd'.

5.3.3 Surface Current Distribution

The simulated surface current distributions on the proposed antenna at different frequencies (0.77 GHz, 1.8 GHz, and3.5GHz) are presented in Fig. 5.8. At 0.77 GHz, the relatively strong current distributions are observed on the shorted L-strip sections. Due to the strong mutual coupling between coupling and radiating strips, the current starts flowing on shorted L-strip section. The capacitive coupling between main radiating elements and parasitic meandered line structure (which is placed on rear side of the substrate) is taken place and due to which the current is also equally concentrated at the meandered strip at lower frequency. The current distribution at 1.8 GHz is illustrated that the strong current distributions at shorting strip. This is because of the resonance appears at 1.8 GHz (as shown in Fig. 5.2). The appearance of resonance at 1.8 GHz confirms that the shorting strip is main contributing structure at this frequency. From the vector current distribution at 3.5 GHz, it is observed that strong current distribution at coupling elements and also at the portion of meandered parasitic which is covered with the coupling elements. The strong current distribution on the coupling strip and back side meandered parasitic is confirmed by (Fig. 5.2) the resonance at 3.5 GHz is due to the coupling elements and end portion of the shorting strip.

5.3.4 Radiation Performances

The simulated and measured radiation patterns of the proposed antenna at different frequencies (0.9 GHz, 1.8 GHz, 2.45 GHz, and 3.5 GHz) in XZ-plane and YZ-plane are plotted in Fig. 5.9. The measured and simulated radiation patterns are observed in agreement. It is observed that in XZ-plane the co-polar patterns show quasi omnidirectional nature at all the frequency points. At low frequency (0.9 GHz) cross-polar level is very low while as the frequency increases the cross polar level rises and become comparable to the co-polar level. In YZ-plane, dumbbell shape co-polar patterns are observed at all the frequencies points and the cross-polar patterns show same behaviour as in the XZ-plane.

The total efficiency is calculated by considering the mismatch losses which is shown in Fig. 5.10. It is observed that the variations of total efficiency lies

between 60 % – 81 % at lower operating bands i.e. LTE700/GSM800/900 (0.742 GHz–1.36 GHz) whereas 54 % – 90 % at the higher frequency bands i.e. GPS L1/GSM1800/1900/UMTS/ IMT2100/Wi-fi/LTE2300/2500 (1.475 GHz–2.7 GHz). At the WiMAX (3.4 GHz–3.72 GHz), the variations of total efficiency is between 13 % – 41 %.

The variations of the peak realized gain is also shown in Fig. 5.10. It is observed that peak realized gain lies between -0.3 dBi to +1 dBi at lower operating bands whereas at higher frequency bands it lies between 0 dBi to -4 dBi.

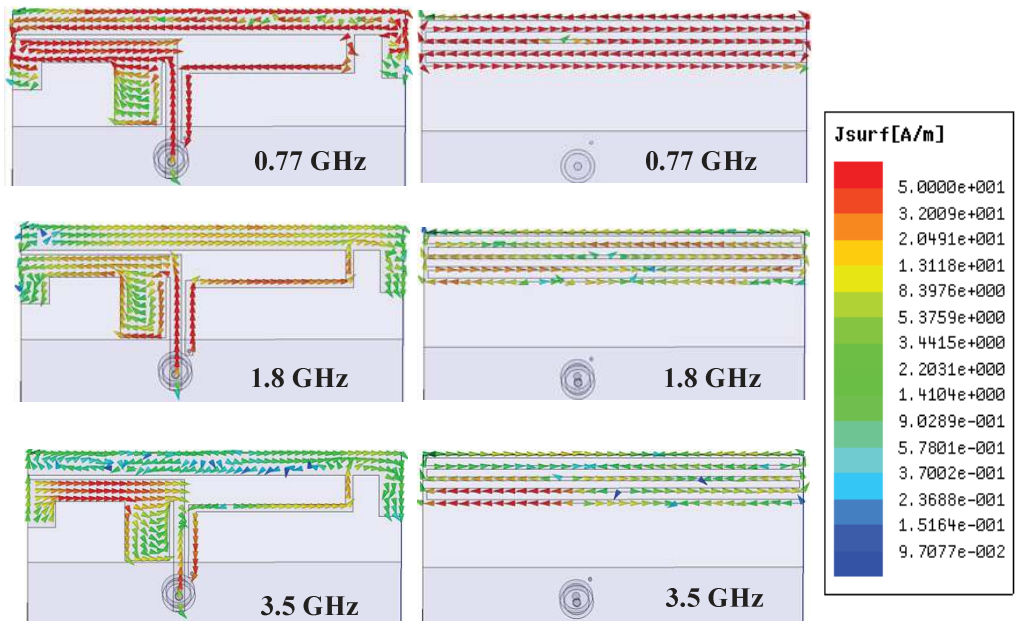

(a) Front view (b) Rear view

Fig. 5.8: Vector surface current distribution at different frequencies.

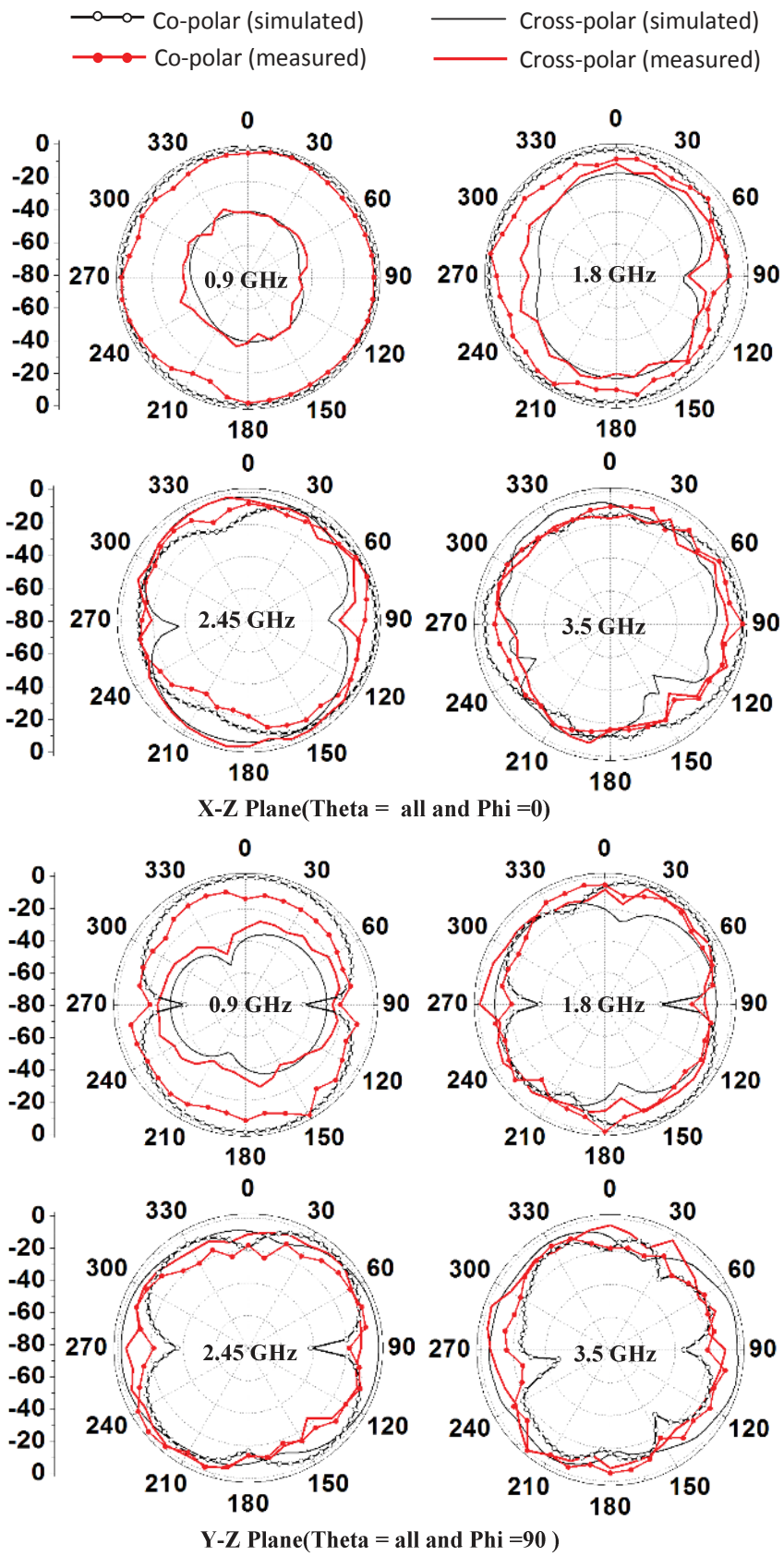

Fig. 5.9: Simulated and measured radiation patterns.

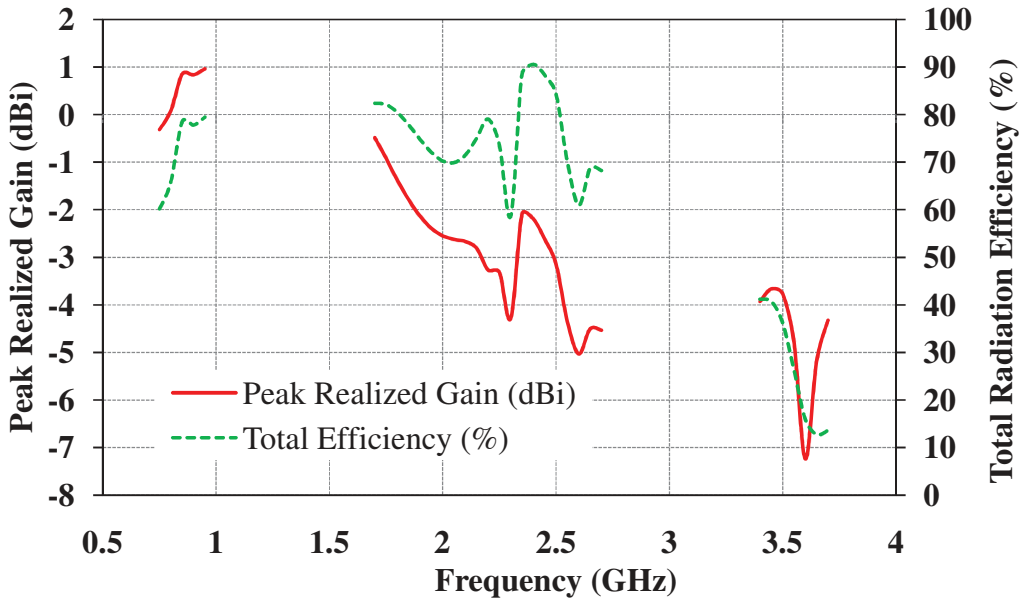

Fig. 5.10: Variation of peak realized gain and total efficiency with frequency.

5.4 Antenna Characterization in Mobile Environment

The proposed antenna is also investigated in the vicinity of the mobile environment. Mobile environment made up with the plastic housing (60×120×14.3 mm^3), LCD display (48×80×2 mm^3), and the battery (33.5×50.5× 4 mm^3). A setup is designed in Ansoft's HFSS as shown in Fig. 5.11. The battery and LCD are assumed as a PEC (perfect electric conductor) material. The LCD placed on the rear side of the substrate (towards ground plane) and battery is placed on the front side of the substrate where antenna is fabricated, and the components have air-gap of 1mm from surface of the substrate. Both the components are connected to the board with metallic connecting pins provided at the ends of the components. Fig. 5.12 shows the variation of reflection coefficient with frequency in free space and in the mobile environment. It is observed that due to the mobile environment mismatch occurred at certain frequencies but still all the operating bands are covered. Therefore, it can be concluded that scattering environment nearby antennas play significant role on the antenna performance. If operating bands are not covered under such scenario, impedance tuning is required in the mobile environment.

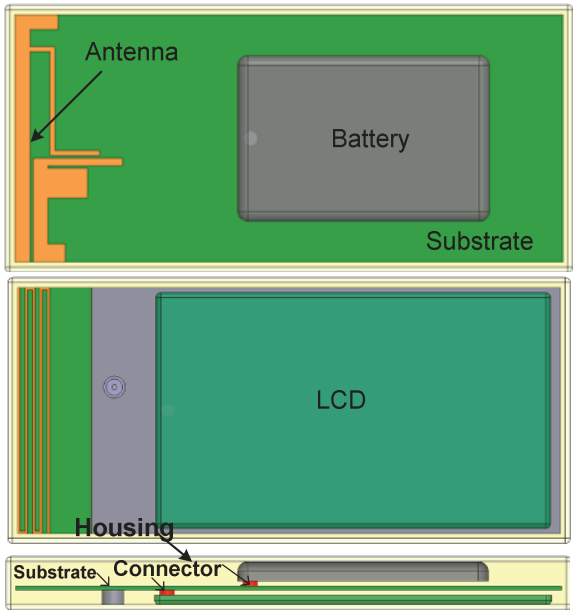

Fig. 5.11: Antenna in mobile environment.

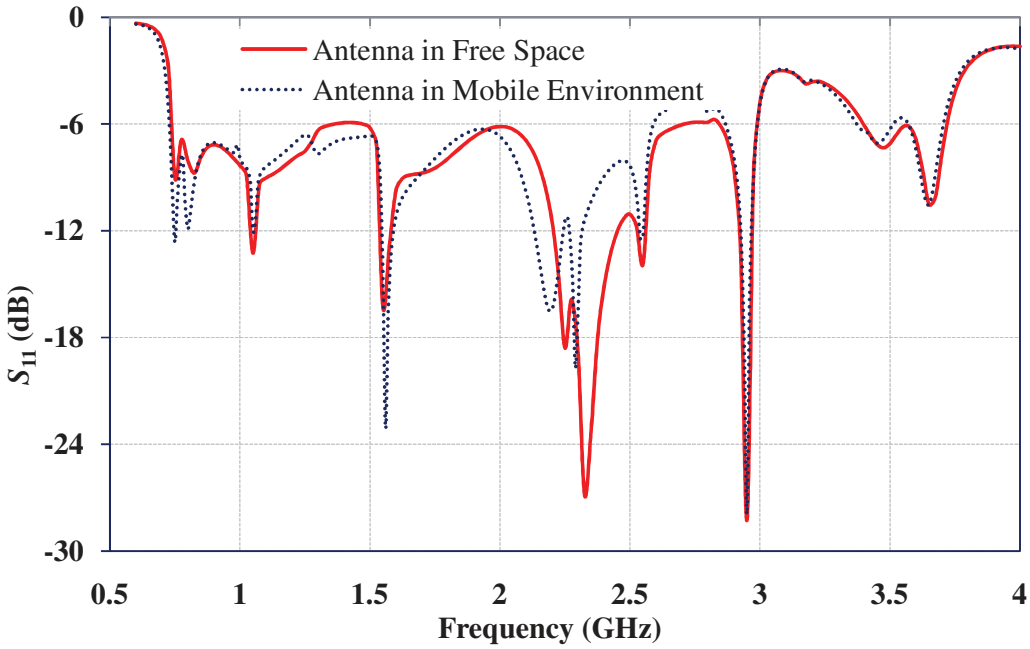

Fig. 5.12: Effect of mobile environment on *S*-parameters.

After investigating the thin profile wideband printed monopole antenna for slim mobile handset applications, all the three antennas proposed in previous chapters are taken up in the next chapter six for the performance study in the vicinity of the user proximity performance.